



1 Geodetic point surface mass balances: A new approach to determine point 2 surface mass balances from remote sensing measurements

3
 4

5 *Christian Vincent¹, Diego Cusicanqui^{1,4}, Bruno Jourdain¹, Olivier Laarman¹, Delphine Six¹, Adrien*
 6 *Gilbert¹, Andrea Walpersdorf², Antoine Rabatel¹, Luc Piard¹, Florent Gimbert¹, Olivier Gagliardini¹,*
 7 *Vincent Peyaud¹, Laurent Arnaud¹, Emmanuel Thibert³, Fanny Brun¹ and Ugo Nanni¹*

8

9 ¹ Université Grenoble Alpes, CNRS, IRD, Grenoble-INP, Institut des Géosciences de l'Environnement
 10 (IGE, UMR 5001), F-38000 Grenoble, France.

11 ² Université Grenoble Alpes, CNRS, ISTERRE, Grenoble, France.

12 ³ Université Grenoble Alpes, INRAE, UR ETGR, Grenoble

13 ⁴ Université Savoie Mont-Blanc, CNRS, Laboratoire EDyTEM, F-73000 Chambéry, France

14

15 Corresponding author: Christian Vincent (christian.vincent@univ-grenoble-alpes.fr)

16

17

18 Abstract

19

20 Mass balance observations are very useful to assess climate change in different regions of the world. As
 21 opposed to glacier-wide mass balances, which are influenced by the dynamic response of each glacier,
 22 point mass-balances provide a direct climatic signal that depends on surface accumulation and ablation
 23 only. Unfortunately, major efforts are required to conduct *in situ* measurements on glaciers. Here, we
 24 propose a new approach that determines point surface mass balances from remote sensing observations.
 25 We call this balance the geodetic point surface mass balance. From observations and modelling
 26 performed on Argentière and Mer de Glace glaciers over the last decade, we show that the vertical ice
 27 flow velocity changes are small in areas of low bedrock slope. Therefore, assuming constant vertical
 28 velocities in time for such areas and provided that the vertical velocities have been measured for at least
 29 one year in the past, our method can be used to reconstruct annual point surface mass balances from
 30 surface elevations and horizontal velocities alone. We demonstrate that the annual point surface mass
 31 balances can be reconstructed with an accuracy of about 0.3 m w.e. a⁻¹ using the vertical velocities
 32 observed over the previous years and data from Unmanned Aerial Vehicle images. Given the recent
 33 improvements of satellite sensors, it should be possible to apply this method to high spatial resolution
 34 satellite images as well.

35



1. Introduction

Glacier surface mass balance observations are widely used to assess climate change in various climatic regimes because of their sensitivity to climate variables [e.g. Zemp et al., 2019; Marzeion et al., 2014; Kaser et al., 2006; Gardner et al., 2013; Huss and Hock, 2018; IPCC, 2019]. *In situ* surface mass balance measurements have been conducted on only a few of the 200,000 mountain glaciers worldwide [WGMS, 2017; Zemp et al., 2015]. In the European Alps, about a dozen annual surface mass balance time series from *in situ* measurements extending over more than 50 years are available [WGMS, 2017]. Recently, considerable efforts have been made to assess ice volume changes at the mountain-range scale over long time periods using geodetic measurements obtained from remote sensing techniques [e.g. Paul and Haeberli, 2008; Abermann et al., 2011; Gardelle et al., 2012; Gardner et al., 2013; Berthier et al., 2014; Brun et al., 2017]. These geodetic methods determine glacier-wide volume changes, or glacier-wide mass balances, by differencing repeated determinations of glacier surface elevations obtained from airborne and spaceborne surveys, usually over multiyear to decadal periods [e.g. Vincent, 2002; Bauder et al., 2007; Soruco et al., 2009; Berthier et al., 2014; Dussaillant et al., 2019]. These methods are effective to estimate the overall glacier mass change and quantify the related hydrological impacts or sea level contribution [e.g. Hock et al., 2005; Kaser et al., 2010; Huss, 2011; Immerzeel et al., 2013; Zemp et al., 2019]. However, the meaningfulness of a climatic interpretation of these results is questionable. Indeed, glacier-wide mass balances are not solely driven by changes in climate but also by changes in glacier geometry controlled by the dynamic response of each glacier [Vincent, 2002; Fischer et al., 2010; Abermann et al., 2011; Huss et al., 2012; Vincent et al., 2017]. Consequently, they do not provide a direct climatic signal. On the other hand, point surface mass balances provide a direct climatic signal which depends only on local accumulation and ablation (Huss and Bauder, 2009; Thibert et al., 2013; Vincent et al., 2004, 2017, 2018b). However, the only way to presently obtain point mass balance data is to make *in situ* measurements. In particular, the net annual ablation in the ablation zone is usually obtained from ablation stakes. These point surface mass balance measurements require huge efforts involving field campaigns and the collection of data from stake measurements scattered over the glacier. This explains why so few *in situ* measurements are performed, especially on glaciers located in remote areas with very difficult access (e.g., Azam et al., 2018; Wagnon et al., 2013; Hoezle et al., 2017).

The objective of this paper is to propose an approach to determine point surface mass balances from measurements obtained by remote sensing techniques. Our aim is to determine point surface mass balances in ablation areas without setting up ablation stakes each year. We will develop this method using a comprehensive dataset of *in situ* measurements and analysis of ice motion, elevation changes and point surface mass balance data in the ablation area of Argentière Glacier (French Alps). We will then validate our method in other areas of the ablation zone of this glacier and of the Mer de Glace glacier.



73

74 2. Study area

75

76 The Argentière Glacier is located in the Mont-Blanc range, French Alps (45°55' N, 6°57'E). Its surface
 77 area was about 12.4 km² in 2003 (Fig. 1). The glacier extends from an altitude of about 3,400 m a.s.l. at
 78 the upper bergschrund down to 1,600 m a.s.l. at the snout. The length of this glacier is about 10 km. It
 79 faces north-west, except for a large part of the accumulation area (south-facing tributaries). The annual
 80 surface mass balance ranges roughly from 2 meters of water equivalent per year (m w.e. a⁻¹) in the
 81 accumulation area to about -10 m w.e. a⁻¹ close to the snout. This glacier is free of rock debris except
 82 for the lowermost part of the tongue, below the ice fall located between 2,000 and 2,300 m a.s.l. The
 83 field observations of the Argentière Glacier (i.e. mass-balance, thickness variations, ice-flow velocities
 84 and length fluctuations over 50 years) come from the French glacier monitoring program called
 85 GLACIOCLIM (Les GLACIers, un Observatoire du CLIMat; <https://glacioclim.osug.fr/>). For the
 86 present study, additional detailed observations were carried out in the framework of the SAUSSURE
 87 program (Sliding of gLACIers and sUbglaial water pressure (<https://saussure.osug.fr/>). The main part of
 88 our study focuses on a small area of Argentière Glacier (~0.2 km²) located at 2,350 m a.s.l. in the
 89 ablation zone (Fig. 1 and 2). In this area, the glacier is ~600 m wide, the horizontal ice flow velocity is
 90 ~55 m a⁻¹ (Vincent and others, 2009) and the maximum ice thickness is 250 m (Rabatel et al., 2018).
 91 Experiments conducted in boreholes (Hantz and Lliboutry, 1983) indicate that the bed is composed of
 92 hard rock with no thick and deforming sediment layer.

93

94 3. Data

95

96 In the selected area, point annual surface mass balances and ice flow velocities were monitored
 97 accurately at the end of each ablation season between 2016 and 2019 from 19 ablation stakes (Fig. 2).
 98 Our study also used surface mass balance and ice flow velocity observations from a small part of the
 99 ablation zone of the Mer de Glace glacier, at the location named “Tacul glacier” (Fig.1).

100 The ablation stakes are 10 meters long and made of five 2-m long sticks tied together with metallic
 101 chains. Errors in ablation measurements mainly come from the mechanical play of the jointed sticks.
 102 The uncertainties of the annual surface mass balance measurements performed in this ablation zone have
 103 been assessed at 0.14 m w.e. a⁻¹ (Thibert et al., 2008). Topographic measurements were performed to
 104 obtain the 3D coordinates of the ablation stakes. For this purpose, we used a Leica 1200 Differential
 105 Global Positioning System (GNSS) receiver, running with dual frequencies. Occupation times were
 106 typically one minute with 1-second sampling and the number of visible satellites (GPS and GLONASS)
 107 was greater than 7. The distance between fixed and mobile receivers was less than 1 km. The DGPS
 108 positions have an intrinsic accuracy of ± 0.01 m. However, given the size of the holes drilled to insert
 109 the stakes, we estimate that the stake positions have an uncertainty of ±0.05 m.



110 The vertical velocity is the vertical component of the surface velocity obtained from stake
111 measurements. It is obtained from the altitude differences of the bottom tip of the stake. In practice, the
112 DGPS measurements are performed simultaneously with the emergence measurements in order to obtain
113 the exact position of the bottom tip of the stake buried in ice. In this way, it is possible to monitor ice
114 velocity along the three coordinate directions. Depending on the tilt of the ablation stakes, the size of
115 the drilling hole and the mechanical play of the jointed stakes, we assume that the annual horizontal and
116 vertical velocities are known with an uncertainty of $\pm 0.10 \text{ m a}^{-1}$.

117 Aerial photographs of the glacier surface were taken on 5 September 2018 and 13 September 2019 using
118 the senseFly eBee+ Unmanned Aerial Vehicle (UAV). A total of 720 photos in 2018 and 673 photos in
119 2019 were collected with the onboard senseFly S.O.D.A. camera (20 Mpx RGB sensor with a 28 mm
120 focal lens from an average altitude of 140 m above the glacier surface). Prior to the survey flights, we
121 collected GNSS measurements of ground control points (GCPs) that consist in rectangular pieces of red
122 fabric (100x60 cm) with white painted circles (40 cm diameter) on the glacier (10 in 2018, 20 in 2019)
123 and ten 40 cm diameter white circles painted on rocks on the sides of the glacier. The original horizontal
124 resolutions of the ortho-photo mosaics and digital elevation models (DEMs) are 10 cm and 1.00 m,
125 respectively. The photos from the survey were processed using the Structure for Motion (SfM) algorithm
126 that is implemented in the Agisoft Metashape Professional version 1.5.2 software package (Agisoft,
127 2019). The SfM stereo technique was then used to generate a dense point cloud of the glacier surface.
128 This dense point cloud was used to construct the DEMs using the GCPs surveyed during the field
129 campaigns. A detailed description of the processing steps can be found in Kraaijenbrink et al. (2016) or
130 Brun et al. (2016).

131 To calculate horizontal ice flow velocities over the studied area, we used the UAV ortho-photo mosaics
132 with COSI-Corr (Co-registration of Optically Sensed Images and Correlation), a software tool
133 developed for image correlation (Leprince et al., 2007; Ayoub et al., 2009). Due to the velocities of the
134 Argenti re glacier in this region ($\sim 55 \text{ m a}^{-1}$), we resampled the UAV ortho-photo at 0.1 m resolution
135 because the correlation was too noisy even with very large window sizes (i.e. 512 pixels). The surface
136 velocities were computed using an initial window size of 256 pixels, a final window size of 64 pixels
137 and a step of 4 pixels. The output velocity field was filtered using signal-to-noise ratios (SNR) provided
138 by COSI-Corr. Using an SNR threshold provides a good compromise between output details, noise and
139 computing time. A detailed description of the correct choice of the window size for correlation can be
140 found in Kraaijenbrink et al. (2016).

141 To establish the possible errors on the correlation process, horizontal displacements on stable off-glacier
142 areas were evaluated and provided a maximum horizontal error of $\sim 0.5 \text{ m}$.

143

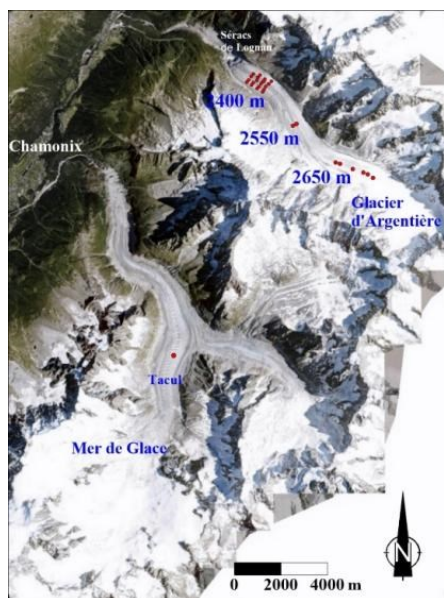


Figure 1: Map of Argentière and Mer de Glace glaciers. The red dots on Argentière glacier are the ablation stakes used in this study for annual surface mass balance and ice flow velocity measurements in 3 regions of the glacier (at approximately 2,400; 2,550 and 2,700 m a.s.l.). Aerial photo from the French National Geographical Institute, 2015 (<https://www.geoportail.gouv.fr/>).

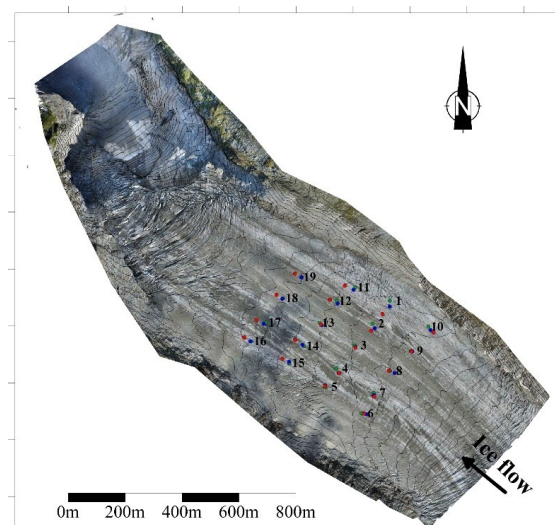


Figure 2: Map of the studied area in the ablation zone of Argentière glacier. The contour lines of surface topography correspond to the surface in 2018. The green, blue and red dots are the positions of the ablation stakes used for surface mass balance and ice flow velocity measurements when they were set up in 2016, 2017 and 2018, respectively. Aerial photo from Unmanned Aerial Vehicle survey (5 September 2018).



4. Method

We will now introduce the mathematical framework used further on.

4.1 Emergence velocities

The emergence velocity is the upward or downward flow of ice relative to the glacier surface. This flow compensates the surface mass balance exactly if the glacier is under steady state conditions. The surface elevation change equation (Cuffey and Paterson, 2010, p. 332) expresses the surface mass balance as a function of surface velocity and surface gradient:

$$b_s = \partial S / \partial t - w_s + u_s \partial S / \partial x + v_s \partial S / \partial y \quad (1)$$

with b_s the surface mass balance expressed in meters of ice, firm or snow (m a^{-1}), S the surface elevation (m), u_s , v_s , w_s the components of ice flow velocity at the surface (m a^{-1}), $\partial S / \partial x$ the surface gradient in the x direction and $\partial S / \partial y$ in the y direction.

The term $w_s - u_s \partial S / \partial x - v_s \partial S / \partial y$ is called the emergence velocity. If the horizontal x-axis is taken in the downslope direction, $v_s = 0$, and the emergence velocity is written as:

$$v_e = w_s - u_s \partial S / \partial x \quad (2)$$

Note that, under steady state conditions, $\partial S / \partial t = 0$ and $b_s = -v_e$. The emergence velocities can be calculated for each ablation stake from horizontal and vertical velocities and the slope of the surface $\partial S / \partial x$. The slope of the surface can be obtained from GNSS field measurements and calculated over a distance similar to that travelled by the stake over one year. In the ablation zone, the emergence velocities are positive, which corresponds to an upward flow of ice relative to the glacier surface. Note also that the vertical velocity can be positive or negative on any region of the glacier. The emergence velocity is a classical way to relate the surface mass balance to the thickness changes (Eq. 1). Unfortunately, as shown later in our study, even if the horizontal and vertical velocities are known accurately, the large uncertainties related to the slope and thickness changes prevent us from calculating the point surface mass balance from the emergence velocities.

At the scale of the year, according to Equation 1 and Figure 3, and considering that the x-axis is taken along the flow line direction (*i.e.*, $v_s = 0$), the annual surface mass balance B_s between the years t and $t+1$ is obtained from:



$$B_s = \Delta h_1 + U_s \tan \alpha_{t+1} - W_s = \Delta h_2 + U_s \tan \alpha_t - W_s \quad (3)$$

192

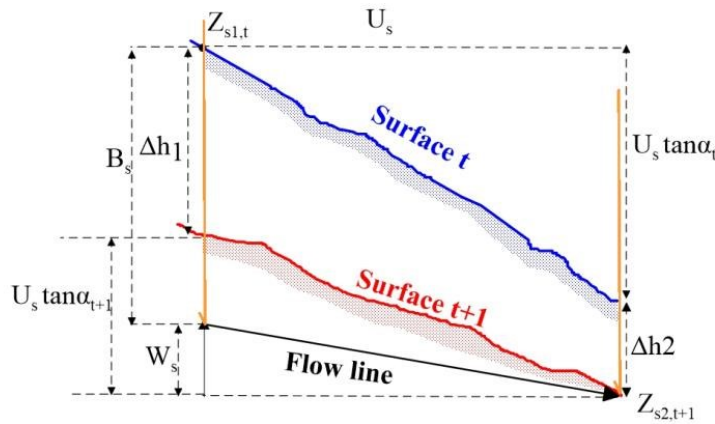
193 where $u_s \cdot \partial S / \partial x$ is replaced by $U_s \tan \alpha_t$ or $U_s \cdot \tan \alpha_{t+1}$ and U_s is the annual surface horizontal velocity and
194 $\tan \alpha_t$ and $\tan \alpha_{t+1}$ are the slopes for the years t and $t+1$ respectively. W_s is the annual vertical velocity.
195 $\partial S / \partial t$ is replaced by Δh_1 and Δh_2 , which are the annual thickness changes observed at the ends of the
196 annual ice flow vector.

197 Figure 3 illustrates the components of Equation 3.

198 Note that the slope of the surface may change from year t to year $t+1$ and the expression depends on the
199 selected slope and thickness changes Δh_1 or Δh_2 (Fig. 3). Obviously, the results are the same.

200

201



202

203 *Figure 3: Diagram illustrating horizontal, vertical and emergence velocities observed from an ablation*
204 *stake (orange). U_s and W_s are the components of horizontal and vertical velocities, α_t and α_{t+1} the slopes*
205 *for the years t and $t+1$ respectively, $Z_{s1,t}$ and $Z_{s2,t+1}$ the elevations of the surface at each end of the ice*
206 *flow vector and Δh_1 and Δh_2 the elevation changes at each end of the ice flow vector.*

207

208 4.2 Calculation of the “geodetic point surface mass balance”

209

210 Let us reconsider the emergence velocity formulation in order to express the point surface mass balance
211 as a function of vertical velocity and altitude changes at the ends of the annual displacement vector.

212 According to Equation 3 and given that $\Delta h_1 + U_s \tan \alpha_{t+1} = \Delta h_2 + U_s \tan \alpha_t = Z_{s2,t+1} - Z_{s1,t}$ (Fig. 3), we
213 can write:

214

$$B_s = Z_{s2,t+1} - Z_{s1,t} - W_s \quad (4)$$

216



This expression has a great advantage in that it does not depend on the surface slope that can change from one year to the next. It is also independent of thickness changes that can change from one site to another.

The term geodetic point surface mass balance refers to the value of B_s obtained from Equation 4. Once the vertical velocity is known, B_s can be obtained from topographical surface measurements alone. Note that even if the horizontal velocity is not included in Equation 4, it is needed to estimate the positions at which $Z_{s2,t+1}$ and $Z_{s1,t}$ should be measured.

5. Results

5.1 Annual horizontal and vertical velocities over the three years

Annual horizontal and vertical velocities were measured from a network of 19 ablation stakes over three years between 2016 and 2019 (Fig. 2). The stakes were replaced each year and were always set up at the same locations, using a handheld GPS device, allowing a relevant comparison, except for stakes 1 and 11 which were located in areas with large crevasses, preventing the possibility of drilling stakes at the chosen location. In addition, for the year 2018/2019, stake 12 was accidentally replaced at a distance of more than 30 meters from the initial position due both to a lack of rigour and to the uncertainty of the handheld GPS instrument. This error led to a bias in the horizontal velocity of 3 m a^{-1} in a region with a strong horizontal gradient (left edge of the area in Figure 4). However, it does not change the pattern of horizontal velocities or horizontal velocity changes with time. This is not the case for vertical velocities as shown below. In the area of this network, the annual horizontal velocities range from 35 to 60 m a^{-1} . The annual ice flow velocities have been interpolated from kriging over the entire coloured areas shown in Figure 4. In this way, we can accurately compare the ice flow velocities over three years, 2016/2017, 2017/2018 and 2018/2019, at the locations of each stake (Fig. 5a). Strong deceleration in horizontal ice flow velocities can be observed over these three years. On the average, ice flow velocity decreased by 2.4 and 1.8 m a^{-1} over the two periods, which corresponds to an average decrease of about 4.8 and 3.6% per year, respectively. Note that the regression lines shown in Figure 5a are almost parallel, which means that the change in velocities is homogeneous in space.

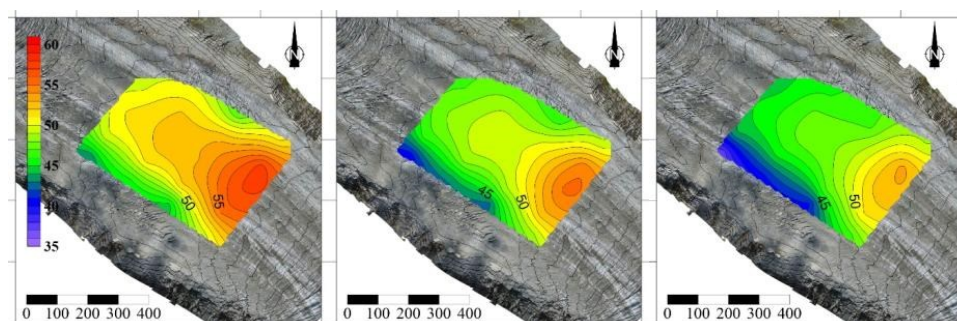
The vertical velocities were obtained from the altitude changes of the bottom tip of the stakes from one year to the next (Fig. 3). In the studied area, the vertical velocities can be positive or negative and range from -4 to 4 m a^{-1} (Fig. 4). The vertical velocities have been interpolated over the entire coloured areas shown in Figure 4 using kriging. The patterns of vertical velocities are very similar for the year 2016/2017 and 2017/2018. We note some differences with the 2018/2019 pattern. As mentioned previously, stakes 1, 11 and 12 set up in 2018/2019 are located at distances of more than 30 meters from the initial positions. In addition, stakes 17, 18, 19 were replaced in 2018 at distances ranging between 25 and 30 meters from the initial positions. These six stakes are shown with small dots in Figure 5b. If



254 we exclude the velocity values of 2018/2019 for these stakes, we can conclude that the measured vertical
255 velocities are very similar over this 3-year period. The differences do not exceed 0.5 m a^{-1} . The average
256 of the differences is 0.01 m a^{-1} and the standard deviation is 0.29 m a^{-1} . These differences barely exceed
257 the measurement uncertainty. Note also that the vertical velocity changes could be affected by the
258 horizontal motion changes or vertical strain rate changes as discussed in Section 6.
259
260

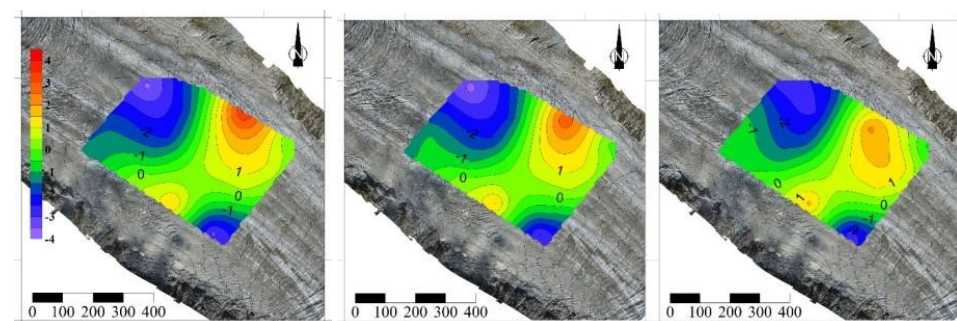


261
 262
 263



2016/2017 2017/2018 2018/2019

264
 265
 266



2016/2017 2017/2018 2018/2019

269

Figure 4: Horizontal (top panel) and vertical (bottom) ice flow velocities (m a^{-1}) measured over three years from the ablation stakes. Note the different colour scales. Distances in m.

270

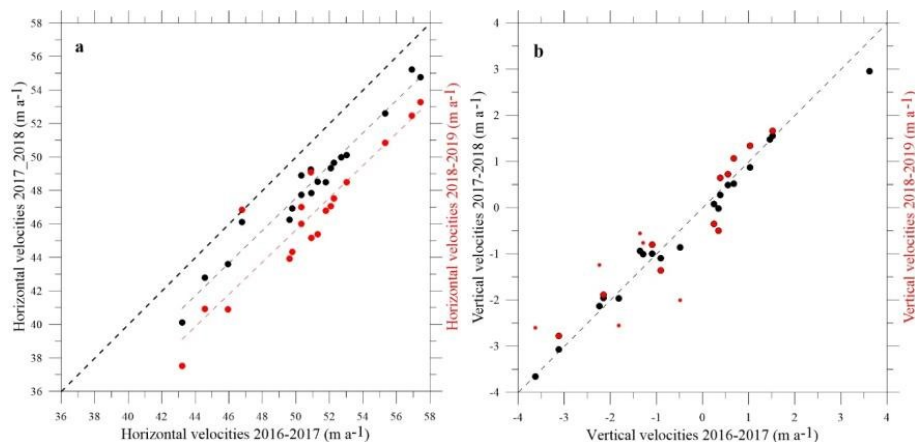


Figure 5: Comparison of horizontal ice flow velocities (a) and vertical velocities (b) between the years 2016/2017, 2017/2018 and 2018/2019. The black dots correspond to the comparison between the



2016/2017 and 2017/2018 periods. The red dots correspond to the comparison between the 2016/2017 and 2018/2019 periods. The thick dashed line corresponds to the bisector and the thin dashed lines to the regression lines. The small dots in the figure on the right correspond to the stakes that were set up in 2018 at distances of more than 25 m from the initial positions.

5.2 Emergence velocities

The emergence velocities have been calculated from Equation 2 for each stake and reported in Figure 6. We compared the emergence velocities obtained each year at each stake location (Fig. 7). Unlike the vertical velocities, the differences between emergence velocities calculated over the 3 years reveal a standard deviation of $0.8 \text{ m w.e. a}^{-1}$. The value of emergence velocities is affected by large uncertainties related to the slope.

Combined with the measured thickness changes, the emergence velocity should make it possible to estimate the surface mass balance. However, our study shows that the uncertainties in the emergence velocity prevent us from calculating the point surface mass balance accurately. Indeed, the dispersion of $0.8 \text{ m w.e. a}^{-1}$ is large compared to the spatial variability of about 1 m w.e. a^{-1} for point surface mass balance in the ablation zone of alpine glaciers (Vincent et al., 2018b).

For this reason, to calculate the surface mass balance, we suggest using the “geodetic point surface mass balance” described earlier rather than the emergence velocity.

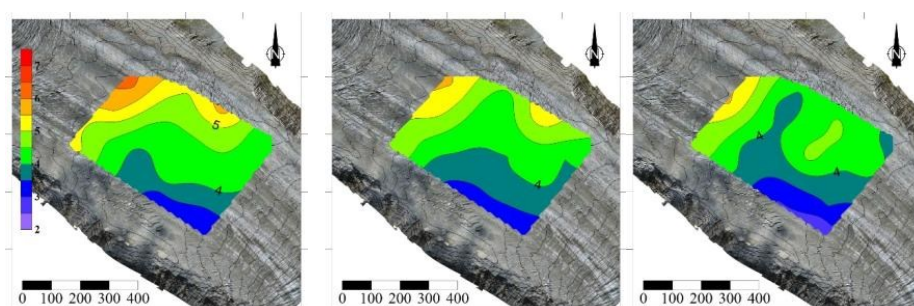


Figure 6: Emergence velocities between the years 2016/2017, 2017/2018 and 2018/2019 (m a^{-1})

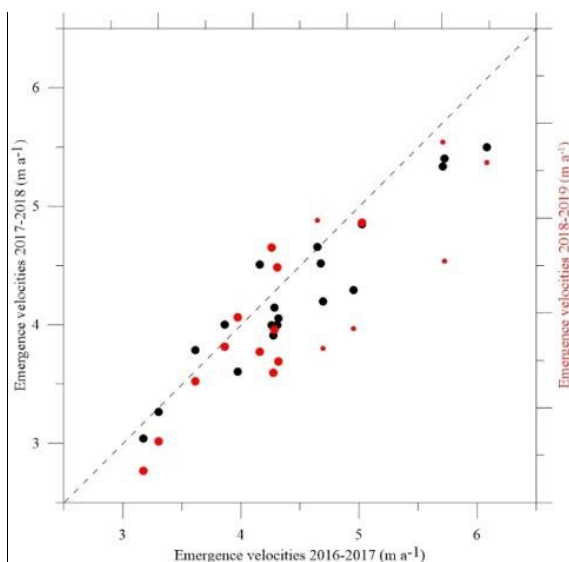


Figure 7: Comparison of emergence velocities between the years 2016-2017, 2017-2018 and 2018-2019. The black dots correspond to the comparison between the 2016-2017 and 2017-2018 periods. The red dots correspond to the comparison between the 2016-2017 and 2018-2019 periods. The red small dots correspond to the stakes that were set up in 2018 at distances of more than 25 m from the initial positions

5.3 “Geodetic point surface mass balances” using *in situ* GNSS measurements

The geodetic point surface mass balance is calculated according to Equation 4. We first tested the method in the studied region of Argentière glacier at 2,400 m a.s.l. using the *in situ* GNSS measurements. For this purpose, we used the altitudes of the surface at the stake locations for the years 2017 and 2018 and the vertical velocities observed in 2016-2017. The resulting point surface mass balances for the hydrological year 2017-2018 are compared with the observed surface mass balance and plotted in Figure 8a. Note that the surface mass balances are in m of ice per year. The comparison shows very good agreement. The maximum difference is 0.39 m of ice per year and the standard deviation is 0.20 m of ice or 0.18 m w.e. per year. In addition, we calculated the surface mass balances of 2018-2019 from the vertical velocities observed in 2016-2017 and 2017-2018 (Fig. 8b). In this case, the comparison with the observed surface mass balances shows large discrepancies. However, a more detailed analysis reveals that the calculated and observed surface mass balances are very similar if the vertical velocities observed in 2016-2017 and 2017-2018 were measured exactly at the same location of the stakes measured in



2018-2019. In Figure 8b, the large dots show the calculated and observed surface mass balances for the stakes located within a distance no greater than 15 m. From this comparison, the differences are less than 0.5 m a^{-1} of ice and the standard deviation is 0.17 m of ice or $0.15 \text{ m w.e. a}^{-1}$. From this analysis, we conclude that the geodetic point surface mass balance can be obtained with an accuracy of about $0.2 \text{ m w.e. a}^{-1}$ using the vertical velocities observed over the previous years. It requires measurement of the horizontal ice flow velocity and the altitudes of the ends of the velocity vector exactly at the same location, within a radius of less than 15 m compared to that of vertical velocity determination. In practice, the vertical velocities should be observed accurately between two years t and $t+1$ from stakes and GNSS measurements. Then, for the following or previous years, the point surface mass balance can be obtained from surface measurements only (without drillings and setting new stakes) using the horizontal velocity and the altitudes of the surface measured at each end of the horizontal vector. In the next section, we examine how such measurements obtained from remote sensing data can also be used effectively to determine the point surface mass balance.

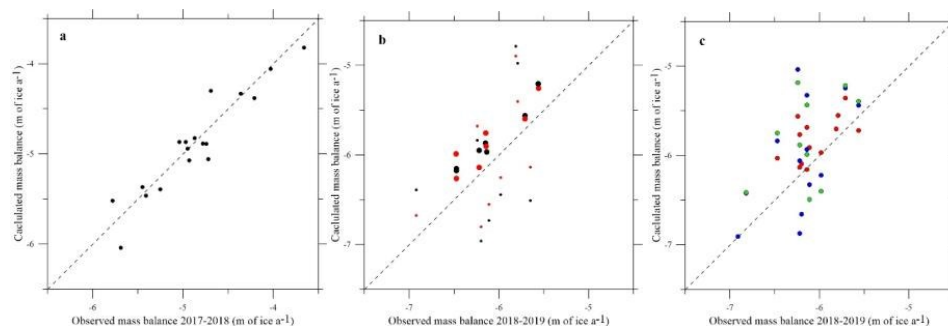


Figure 8: Observed and calculated point surface mass balances at 2,350 m a.s.l. at Argentière glacier. The point surface mass balances have been calculated: a) for the year 2017-2018 using the vertical velocities measured in 2016-2017 and elevations from GNSS measurements; b) for the year 2018-2019 using the vertical velocities measured in 2016-2017 (black dots) and 2017-2018 (red dots), and elevations from GNSS measurements; c) for the year 2018-2019 using elevations from remote sensing data (UAV data) and the vertical velocities measured in 2018-2019 (red dots), 2017-2018 (blue dots) and 2016-2017 (green dots). The large dots shown in Figure 8b correspond to the stakes which were set up within a radius of less than 15 m.



5.4 “Geodetic point surface mass balances” using remote sensing measurements

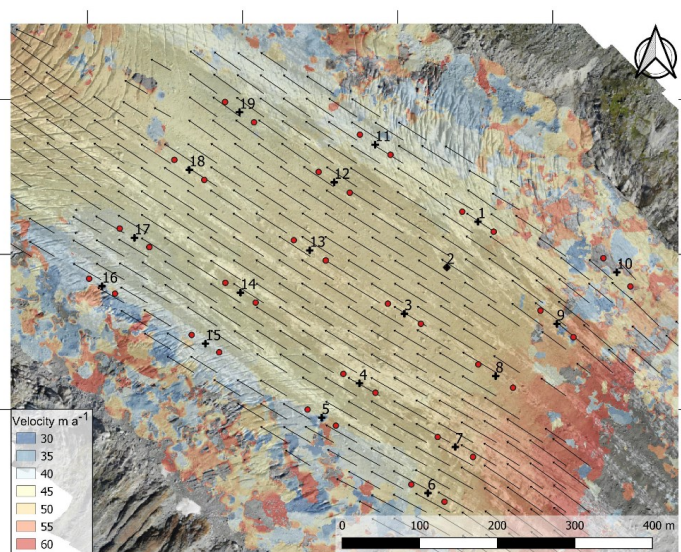
Here, we used the same method described in the previous section. However, the *in situ* GNSS measurements used to determine the altitudes and horizontal velocities are replaced by remote sensing measurements. For this purpose, we used the horizontal velocities (Figure 9) and the DEMs (Figure 10) obtained from UAV surveys in 2018 and 2019. The vertical velocities are those observed in 2018-2019, 2017-2018 and 2016-2017. The horizontal velocities have been neglected for stakes 9 and 10 given the poor quality of the correlation and the opening and/or closing of crevasses in the ice (close to the stake 10) that caused a drastic change between the photos, which subsequently affected the image correlation (Fig. 9).

Some details on the procedure are given below for the sake of clarity. The horizontal velocities retrieved from the UAV surveys were determined at positions where vertical velocities were measured. In this way, the coordinates XY of each vector end have been calculated (green dots on Fig. 9). Then we used the DEMs from 2018 and 2019 to determine the elevations of these points $Z_{s1, 2018}$ and $Z_{s2, 2019}$ (see Eq. 4 and Figure 3). The comparison between the *in situ* horizontal velocities and the velocities obtained from the UAV surveys reveals a standard deviation of 0.7 m a^{-1} .

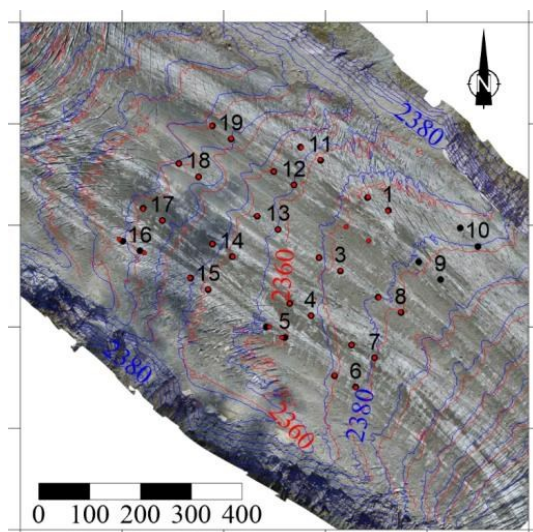
The reconstructed point surface mass balances are compared with the observed surface mass balances in Figure 8c. For this reconstruction, we used the vertical velocities observed in 2018-2019 (red dots), 2017-2018 (blue dots) and 2016-2017 (green dots). For the reconstructions using the vertical velocities of 2016-2017 and 2017-2018, we excluded data of sites 1, 11, 12, 17, 18 and 19 for which the stakes were measured at distances of more than 30 m from those of 2018-2019.

The differences between the observations and the reconstructed surface mass balances using the 2018-2019 vertical velocities are less than 0.45 m of ice per year and the standard deviation is 0.24 m of ice or $0.22 \text{ m w.e. a}^{-1}$. The differences between the observations and the reconstructed surface mass balances using the 2016-2017 and 2017-2018 vertical velocities show standard deviations of 0.42 and 0.40 m w.e. a^{-1} , respectively.

From these results, we conclude that the point surface mass balances can be obtained with an accuracy of about $0.3 \text{ m w.e. a}^{-1}$ using remote sensing measurements, assuming that the vertical velocities have been observed accurately over the previous years.



381
 382 *Figure 9: Horizontal velocities obtained from feature tracking (Cosi-Corr) using UAV images. The*
 383 *black crosses show the locations where the vertical velocities were observed. The red dots correspond*
 384 *to the ends of horizontal vectors for 2018-2019, determined from UAV images.*
 385



386
 387
 388 *Figure 10: DEMs obtained from the UAV survey in 2018 (blue contour lines) and 2019 (red contour*
 389 *lines). The black dots correspond to the positions of the stakes in 2018 and 2019 observed from GNSS*
 390 *measurements. The red dots correspond to the ends of the horizontal velocity vectors obtained from*
 391 *UAV images.*



5.5 Validation of the method: geodetic surface mass balances obtained in other regions

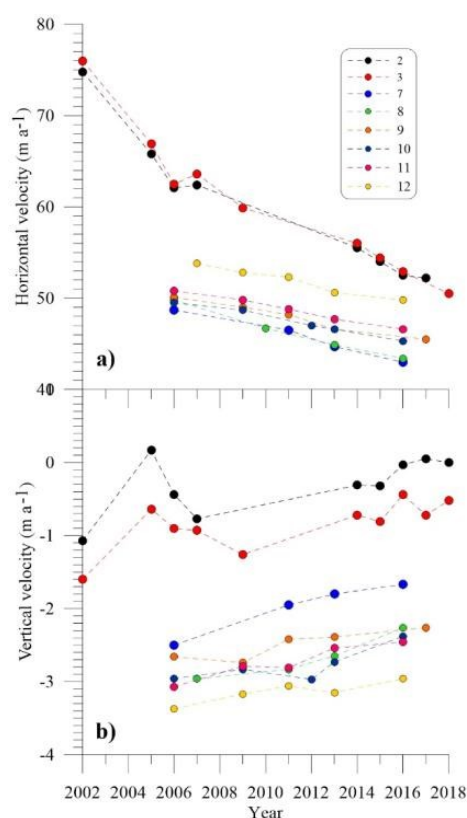
In order to establish that the results are neither accidental nor site-dependent, we tested the method on other areas of Argentière glacier and on another glacier: the Mer de Glace, approximately 10 km away (Fig. 1), for which vertical velocities were available. Here, we used GNSS *in situ* measurements given that accurate elevations observations from remote sensing data are not available.

First, we selected two ablation stakes in a sector of Argentière glacier located at 2,530 m a.s.l. These stakes were replaced within a radius of ± 35 m each year between 2001 and 2018 (Fig. 1). Note that these measurements were not intended for vertical velocity determination but rather for point surface mass balance measurements. This explains why the stakes were not set up at exactly the same locations over the whole period. Note also that the region is not debris-covered and consequently the surface roughness is lower compared to the studied area at 2,350 m. Using Equation 4 and the method described in the previous section, we calculated the point surface mass balances at these two stakes over the period 2001-2018. For this purpose, we used the average vertical velocities calculated over this period and the altitudes of each stake for each year of this period. These two stakes (named stake 2 and stake 3) are located about 120 m apart. The average calculated vertical velocities are -0.24 m a^{-1} ($\pm 0.44 \text{ m a}^{-1}$) and -0.79 m a^{-1} ($\pm 0.33 \text{ m a}^{-1}$), respectively, and did not show strong temporal changes (Fig. 11b). Note that the horizontal velocity decreased from 75 to 50 m a^{-1} in this region between 2002 and 2018 (Fig. 11a). The geodetic point surface mass balances are compared to the observations (Fig. 12a). The standard deviations of the calculated and observed surface mass balance differences are similar to those of the vertical velocities (0.44 and 0.33 m a^{-1} , i.e. 0.4 and 0.3 m w.e. a^{-1}).

Second, we tested the method in another sector of Argentière glacier, close to the equilibrium line, which is located close to 2,800 m a.s.l. For this purpose, we selected 6 stakes (stakes 7, 8, 9, 10, 11, 12) which were measured along a longitudinal section between 2,650 and 2,750 m a.s.l. (Fig. 1) over the period 2005-2018. In this region, the horizontal ice flow velocity is about 50 m a^{-1} (Fig. 11a). Here again, the network of stakes was mainly designed for point surface mass balance measurements. Thus, given that the stakes were set 10-m deep in the ice and the surface mass balance ranges between -4 and 0 m w.e. a^{-1} depending on the year, the ablation stakes were not replaced each year. As the ablation stakes move with the ice flow, we selected only the measurements that were performed at the same locations. Indeed, after the first year following installation, the location of each stake was far from its initial position and we cannot assume that the vertical velocity was similar. Consequently, 5 years are available to calculate the vertical velocities and to make the comparison between calculated and observed point surface mass balances (Fig. 12b). The standard deviations of calculated and observed point surface mass balance differences are 0.22 m of ice a^{-1} , i.e. 0.20 m w.e. a^{-1} .



428 Finally, we tested the method on another glacier, Mer de Glace (Fig. 1). On this glacier, we selected
429 one stake at 2100 m a.s.l that was measured over 15 years between 2003 and 2018 (Vincent et al.,
430 2018a). This ablation stake was set up each year at the same location, within a radius of about 30 meters.
431 Using the method described in the previous sections, we calculated the point surface mass balances at
432 this stake over the period 2003-2018. The average calculated vertical velocity is -1.10 m a^{-1} . Note that
433 the horizontal velocity decreased from 80 to 50 m a^{-1} and the thickness by 55 m in this region between
434 2003 and 2018. The results are plotted in Figure 12c. The standard deviation of the calculated and
435 observed point surface mass balance differences is $0.40 \text{ m w.e. a}^{-1}$.
436



437
438 Figure 11: Horizontal (a) and vertical (b) velocities observed at the different stakes at 2,550 m a.s.l. (Stakes 2 and
439 3) and 2,700 m a.s.l. (stakes 7, 8, 9, 10, 11 and 12).
440

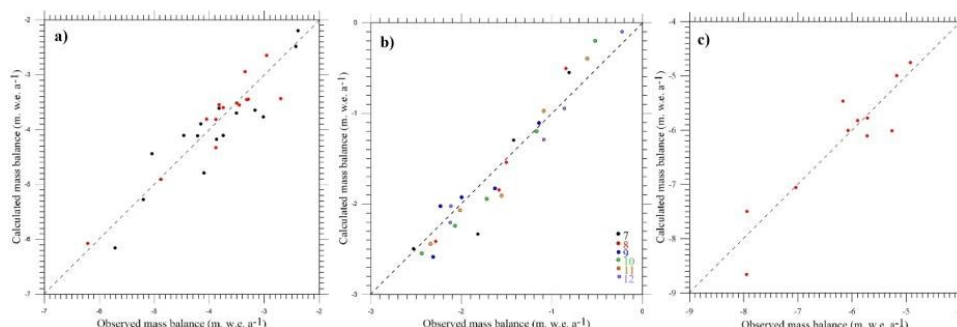


Figure 12: Observed and calculated point surface mass balances from: a) two ablation stakes located at 2,550 m a.s.l. at Argentière glacier measured between 2002 and 2018, b) six stakes located at around 2,700 m a.s.l. at Argentière glacier measured between 2006 and 2017 and c) one stake located at 2,100 m a.s.l. on Mer de Glace glacier measured between 2003 and 2018.

6. Discussions

6.1 Point surface mass balance obtained from emergence velocities vs. vertical velocities

A classical approach to relate the point surface mass balance to thickness change is to use the emergence velocity (Cuffey and Paterson, 2010; Kaab and Funk, 1999). From this approach, the point surface mass balance is obtained from the sum of the emergence velocity and the thickness change (Eq. 1). However, the value of the mass balance reconstructed from the emergence velocity depends strongly on the selected surface slope and on thickness change, which both vary considerably with space and time. The value of the slope depends on the choice of the selected distance for the slope calculation and on the roughness of the surface.

In addition, the slope can change significantly from one year to the next. The emergence velocity is therefore not well-defined given that it depends strongly on the spatial and temporal changes of surface roughness, preventing an accurate determination of point surface mass balance as shown in our study.

In contrast, in our analysis, we find that the vertical velocity is almost constant from year to year, at least at a decadal time scale. Thus, we propose to reformulate the emergence velocity formulation (Eq. 1) in order to express the point surface mass balance as a function of vertical velocity and altitude changes at the ends of the annual displacement vector (Eq. 4). In this way, provided that the vertical velocity has been assessed from *in situ* measurements over previous years, the point surface mass balance can be determined from remote sensing measurements alone, outside the period of field measurements. Our results from the detailed studied area at Argentière glacier (2,350 m a.s.l.), for which the observations were designed to accurately determine the vertical velocity, demonstrate that the surface mass balance can be obtained from this method with an accuracy of about 0.2 m w.e. a⁻¹ from *in situ* GNSS



measurements and about 0.3 m w.e. a^{-1} using elevations and horizontal velocities obtained from very high resolution remote sensing data acquired from UAV surveys.

6.2 Spatial and temporal variability of the vertical velocities

Our dataset shows that the spatial variability of vertical velocities can be large and strongly varies depending on the considered area at the glacier surface. For instance, we found strong spatial variability in the vertical velocity pattern at 2,350 m a.s.l. on Argentière Glacier. Our data suggest that the vertical velocity spatial gradient can reach 1.5 m $a^{-1}/100$ m in this region. As a consequence, a horizontal deviation of 10 m could lead to a vertical velocity change exceeding the measurement uncertainty (0.15 m a^{-1}). Despite this strong spatial variability, we found small changes in vertical velocities with time. Below, we discuss the results of a numerical experiment conducted on Argentière Glacier to understand why.

To analyse the spatial and temporal variabilities of the vertical velocities over the entire glacier, we performed 3D full-Stokes ice-flow simulations for two different glacier geometries using a surface DEM measured in 1998 and 2015 and reconstructed bedrock topography (Rabatel et al., 2018). The calculation is solved using the Elmer/Ice model (Gagliardini et al., 2013). The linear basal friction parameter is inferred from surface velocity and topography measurements made in 2003 (Berthier et al., 2005) using the adjoint-based inverse method (Gillet-Chaulet et al., 2012). For each given glacier geometry, we compute the corresponding flow solution and assume constant friction over time. Therefore, changes in velocity are only induced by changes in the glacier geometry between 1998 and 2015. We used an unstructured mesh with a 100 m horizontal resolution, refined down to 10 m in the stake network monitoring area at 2,400 m a.s.l.

By integrating the mass conservation equation for an incompressible fluid along the vertical axis we can write:

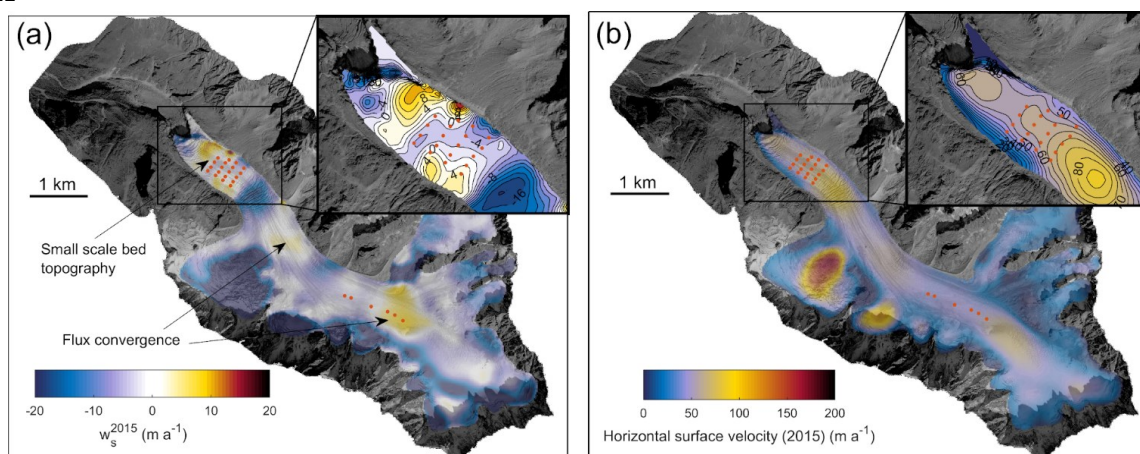
$$w_s = w_b - \int_{z_b}^{z_s} \frac{\partial u}{\partial x} + \frac{\partial v}{\partial y} dz \quad (5)$$

where w_b is the vertical velocity at the bed, z_s is the surface elevation and z_b the bed elevation. Vertical velocity at the surface can therefore be viewed as a sum of a component coming from sliding along the bedrock and a component coming from convergence/divergence of the ice flow integrated over the glacier thickness. For example, local depression in the bedrock topography creates negative vertical velocity w_b at the glacier base but also flow convergence that creates positive vertical velocity resulting in a smoothing of surface vertical velocity w_s by the ice deformation. Figure 13a shows the modelled vertical surface velocity in 2015. At the scale of the glacier, vertical surface velocities are spatially heterogeneous due to a combination of bedrock slope and the ice flux divergence/convergence (Fig. 13a). In the model, the basal vertical velocity w_b produced by ice flow along the bedrock can lead to



small scale variability of the basal vertical velocity that can be visible at the surface when sliding velocity is significant, as modelled around 2,400 m a.s.l. in the studied stake network (Fig. 13a). Bedrock topography is therefore likely the origin of the observed pattern at 2,400 m a.s.l. (Fig. 4). The pattern differences between the observations and the modelling results are likely due to bedrock elevation errors. Although the pattern of horizontal velocities is well reproduced (Fig. 13b), it seems difficult to perfectly reconstruct the vertical velocities.

512



513

514 *Figure 13 – Vertical (a) and horizontal (b) surface velocities modelled at Argentière glacier in 2015.*
 515 *Red dots show the locations of the ablation stakes set up at 2,400 m and 2,650 m a.s.l.*

516

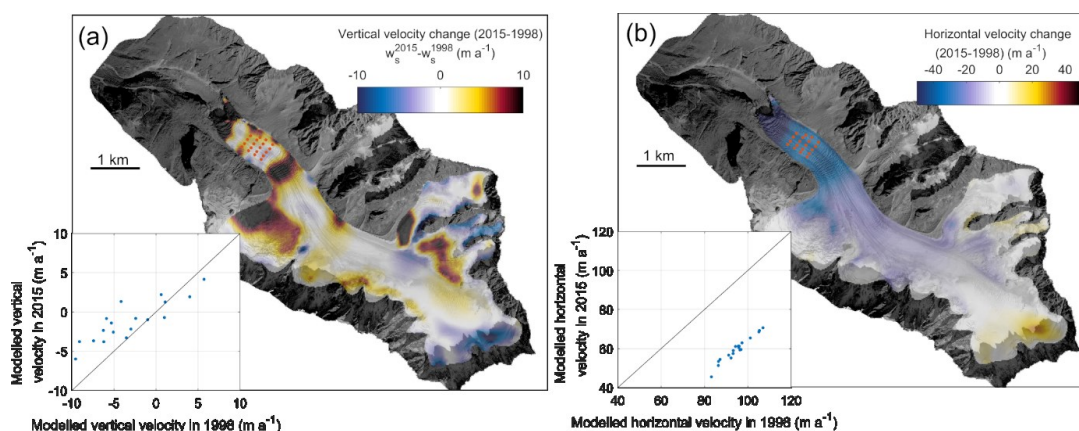
Our numerical experiments were used to analyse the temporal changes in vertical velocities. We found that the response of the vertical velocities at the glacier surface to changes in glacier thickness over time is sensitive to the bedrock slope (averaged over a distance greater than the ice thickness). Consequently, a decreasing vertical velocity magnitude should be associated with decreasing horizontal velocities where bed slopes are significant (Fig. 14). However, the magnitude of small scale (length-scale inferior to glacier thickness) spatial variations of vertical velocity due to bedrock topography seems to be little affected by the large change in horizontal velocities (Fig. 14 and 15). We show that reduced amplitude of w_b due to decreasing sliding speed is compensated by the reduced amplitude of the ice flux convergence/divergence produced by bedrock anomalies (red arrows in Fig. 15). Bedrock depressions and bumps of sizes comparable to glacier thickness produce respectively convergence and divergence in the ice flow, creating vertical velocities of opposite sign compared to the velocities created by sliding at the glacier base. These two components of the surface vertical velocity decrease in magnitude in response to thickness changes, resulting in a limited change in the sum of the two components and therefore in surface vertical velocities. This results in nearly constant vertical velocity where large scale



531 averaged bedrock slope is low, which explains why the observed pattern of surface vertical velocity
532 (Fig. 4) is well conserved over time.

533

534



535

536 *Figure 14: Modelled changes in vertical (a) and horizontal (b) surface velocities between 1998 and*
537 *2015. Insets compare modelled velocities at the stake location (orange dots) between 1998 and 2015.*

538

539 In summary, at large scale, the magnitude of surface vertical changes over time are proportional to
540 bedrock slope and changes in horizontal velocities while at small scale, the spatial patterns tend to be
541 conserved over time due to compensation between changes in bedrock vertical velocities and ice flux
542 convergence/divergence. These findings suggest that our method is likely applicable only in areas of
543 low bedrock slope.

544

545

546

547

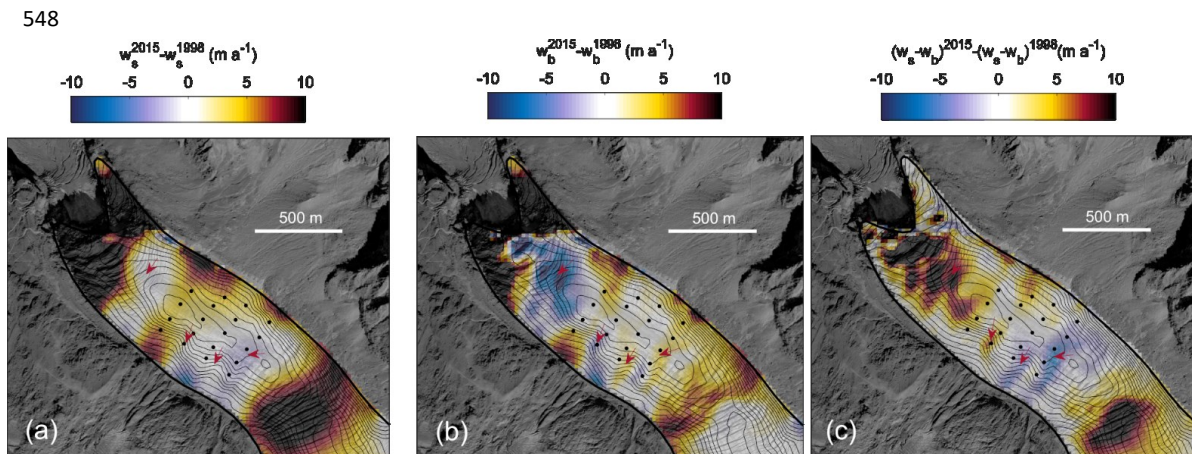


Figure 15: Modelled changes in vertical velocities at the surface (a) and at the bedrock (b) between 1998 and 2015. The right hand figure (c) shows the change in vertical velocity at the surface due to change in flow convergence/divergence. The red arrows indicate the locations where changes in basal vertical velocities are compensated by flow convergence/divergence changes, resulting in constant surface vertical velocities.

Note that, in our study, we used the annual velocities from September to September. Many studies pointed out seasonal changes of the vertical and horizontal motion and possible basal uplift and bed separation (e.g. Sugiyama et al, 2004; Nienow et al., 2005). Here, we assume that these changes do not influence the annual velocities. In our study, the point surface mass balances and vertical velocities have been measured at the end of the ablation season. As a consequence, the geodetic annual surface mass balances obtained from the vertical velocities should not be affected by seasonal changes.

6.3 Uncertainties on geodetic point surface mass balances

The uncertainty related to the point surface mass balance determination results from the uncertainties on the elevation measurements and on the vertical velocity. Using Equation 4 and assuming independence of the different sources of uncertainties, the overall uncertainty related to the reconstructed point surface mass balance is obtained by applying the method of error propagation and assuming uncorrelated errors:

$$\sigma_b^2 = 2\sigma_z^2 + \sigma_w^2 \quad (6)$$

in which σ_b , σ_z , σ_w are the uncertainties relative to the point surface mass balance, elevation and vertical velocity, respectively.



574 The uncertainty in elevation depends both on the method of XY positioning, the surface slope or
575 roughness and the method of altitude determination. Depending on the surface roughness, we can assess
576 the elevations with an accuracy ranging from 0.1 to 0.3 m from UAV measurements as shown in this
577 study.

578 The uncertainty in vertical velocity is $\pm 0.1 \text{ m a}^{-1}$, as mentioned in the Data section. However, additional
579 uncertainty could come from the method of elevation observations for the bottom of the stakes. Indeed,
580 the GNSS measurements are commonly related to the surface of the ice at the location of the stakes and
581 not to the summit of the stakes. Consequently, the altitude of the bottom of each stake results from the
582 difference between the altitude of the surface and the buried height of the ablation stake. Indeed, this
583 determination is accurate only if the measurement of emergence has been performed exactly from the
584 point on which the GNSS measurement was made. Unfortunately, in most cases, one operator held the
585 stick of the GPS antenna at the ice surface close to the ablation stake and another operator measured the
586 emergence of the stake, but not exactly from the surface altitude that corresponds to the bottom tip of
587 the GPS antenna. Except for the measurements performed at 2,350 m a.s.l between 2016 and 2019,
588 which were designed for this purpose, this gives an additional uncertainty of $\pm 0.1 \text{ m}$ for the altitude of
589 the bottom of the stake, *i.e.* $\pm 0.14 \text{ m a}^{-1}$ for the calculated vertical velocity.

590 The overall uncertainty in the geodetic point surface mass balance obtained from remote sensing data is
591 therefore estimated to range between ± 0.20 and $\pm 0.60 \text{ m a}^{-1}$ using accurate DEMs from UAV
592 photogrammetry.

593

594

595 7 Conclusions

596 The classical way to determine the point surface mass balance in the ablation zone of a glacier is to set
597 up ablation stakes and dig pits or conduct drillings in the accumulation zone.

598 Here, we showed that, in the ablation zone, the point surface mass balances can be reconstructed from
599 surface altitudes and horizontal velocities only, provided that the vertical velocities have been measured
600 for at least one year in the past. Our method first requires accurate measurement of the vertical velocities
601 between two years t and $t+1$ from stakes and GNSS measurements. Then, for the following or previous
602 years, the point surface mass balances can be obtained easily from surface measurements only, using
603 the horizontal velocity and the surface elevation at each end of the horizontal displacement vector (Eq.
604 4). These measurements can be obtained from remote sensing provided that the ice flow velocity and
605 altitude determinations are sufficiently accurate.

606 Our method assumes that the annual vertical velocities are almost constant with time. We have used a
607 numerical modelling study to show that this approximation holds in areas of low bedrock slope
608 (averaged averaged over a distance greater than the ice thickness). This is supported by our detailed
609 observations performed on Argenti re Glacier at 2,400 m a.s.l. and designed for this purpose.
610 Comparison between the reconstructed point surface mass balances and the observed values shows close



611 agreement. From our results, we conclude that the point surface mass balances can be obtained with an
612 accuracy of about 0.3 m w.e. a^{-1} using remote sensing measurements and assuming that the vertical
613 velocities have been observed accurately over the previous years. Note that the measurement uncertainty
614 related to the *in situ* measurements of point surface mass balance is 0.14 m w.e. a^{-1} in the ablation zone
615 (Thibert et al., 2008).

616 Further tests performed on dataset in other regions of the Argentière and Mer de Glace glaciers show
617 standard deviations of ± 0.2 to ± 0.4 m w.e. a^{-1} between reconstructed and observed point surface mass
618 balances, despite the fact that these measurements were not designed for this purpose. For these tests,
619 we used the averaged vertical velocities obtained over the last decade.

620 Given the recent improvements in satellite sensors, it is conceivable to apply our method using high
621 spatial resolution satellite images like Pléiades or WorldView (0.5 m resolution). For these point surface
622 mass balance reconstructions, note that, given the strong spatial variability of vertical velocity, it is
623 crucial to determine the altitudes of the surface at each end of the horizontal displacement vector at the
624 exact sites on which the vertical velocities are known. We conclude that our method could be useful to
625 determine numerous point surface mass balances and reduce the amount of effort required to conduct
626 field measurements, especially in remote areas.

627 Previous studies have shown that the point surface mass balance signal reveals a climatic signal that is
628 unbiased by the dynamic glacier response, unlike the commonly used glacier-wide mass balance
629 (Rasmussen, 2004; Huss et al., 2009; Eckert et al., 2011; Thibert et al., 2018; Vincent et al., 2017). In
630 the glaciological community, there is growing awareness that point surface mass balance measurements
631 are important basic data to be shared for mass balance and climate change analyses. In this respect, the
632 World Glacier Monitoring Service has started collecting such data on a systematic basis as a complement
633 to glacier-wide surface mass balances [WGMS, 2015]. Our method should open up new prospects to
634 obtain more numerous point surface mass balances in the future while reducing the amount of time and
635 energy required for *in situ* measurements.

636 Another line of research, not explored in the present study, could also be examined. The method
637 proposed in the present study requires the vertical velocity to reconstruct the annual point surface mass
638 balance. However, if we derive Equation 4 and assume that vertical velocity is constant with time, we
639 can determine the surface mass balance changes, instead of the absolute surface mass balances, with the
640 elevation determinations only. Assuming that satellite sensors provide sufficient accuracy in elevation
641 and horizontal velocity, this method could be very helpful to reconstruct changes in surface mass balance
642 in remote areas for which *in situ* measurements are very difficult. In this way, point surface mass balance
643 changes on numerous unobserved glaciers could be considered with remote sensing observations only.
644 This would make it possible to obtain climatic signals all over the world, unbiased by dynamic glacier
645 response.

646



647 **Data availability:** The surface mass balance, ice flow velocities and DEM data can be accessed upon
 648 request by contacting Christian Vincent (christian.vincent@univ-grenoble-alpes.fr).

649

650 **Author contributions:** DC, OL, DS, BJ, LA, UN, AW, LP, OG, VP, ET, FB and CV performed the
 651 topographic measurements (photogrammetry, lidar, GNSS). OL, DC, AG, FG, OG, FB and CV
 652 performed the numerical calculations and the analysis. AG performed the numerical modelling
 653 calculations. CV supervised the study and wrote the paper. All co-authors contributed to discussion of
 654 the results.

655

656 **Competing interests:** the authors declare that they have no conflict of interest.

657

658 Acknowledgments

659 This study was funded by *Observatoire des Sciences de l'Univers de Grenoble* (OSUG) and *Institut des*
 660 *Sciences de l'Univers* (INSU-CNRS) in the framework of the French GLACIOCLIM (*Les GLACIers,*
 661 *un Observatoire du CLIMat*) program. This study was also funded by *l'Agence Nationale de la*
 662 *Recherche* in the framework of the SAUSSURE program (Sliding of glAciers and sUbglaial water
 663 pressure (<https://saussure.osug.fr>) (ANR 18 CE1 0015 01). IGE and ETGR are part of LabEx
 664 OSUG@2020 (Investissements d'avenir – ANR10 LABX56). We thank all those who conducted the
 665 field measurements. We are grateful to H. Harder for reviewing the English.

666

667 References

668 Abermann, J., Kuhn, M., and Fischer, A. : Climatic controls of glacier distribution and glacier changes in
 669 Austria, *Ann. Glaciol.*, 52, 83–90, 2011.

670

671 Agisoft, Metashape Professional Edition, Version 1.5. Agisoft LLC St Petersburg, 2019.

672

673 Ayoub, F., Leprince, S. and Keene, L. : *User's guide to COSICORR co-registration of optically sensed*
 674 *images and correlation*. California Institute of Technology, Pasadena, CA, 2009.

675

676 Azam M.F., Wagnon, P., Berthier, E., Vincent, C., Fujita, F. and Kargel, J. S.: Review of the status and
 677 mass changes of Himalayan-Karakoram glaciers, *J. of Glaciology*, doi: 10.1017/jog.2017.86, 2018.

678

679 Bauder A., Funk, M. and Huss, M. : Ice volume changes of selected glaciers in the Swiss Alps since the
 680 end of the 19th century. *Ann. Glaciol.*, 46, 145-150, 2007.

681



- 682 Berthier, E., Vadon, H., Baratoux, D., Arnaud, Y., Vincent, C., Feigl, K., and Rémy, F. : Surface motion
683 of mountain glaciers derived from satellite optical imagery, *Remote Sens. Environ.*, vol. 95, n°1, 14-28,
684 2005.
- 685
- 686 Berthier, E., Vincent, C., Magnússon, E., Gunnlaugsson, Á. Þ., Pitte, P., Le Meur, E., Masiokas, M., Ruiz,
687 L., Pálsson, F., Belart, J.M.C., and Wagnon, P. : Glacier topography and elevation changes from Pléiades
688 sub-meter stereo images, *The Cryosphere*, 8, 2275–2291, doi:10.5194/tc-8-2275-2014, 2014.
- 689
- 690 Brun, F. and 9 others : Quantifying volume loss from ice cliffs on debris-covered glaciers using high
691 resolution terrestrial and aerial photogrammetry, *J. Glaciol.*, 62(234), 684-6951-12, doi
692 10.1017/jog2016.542016, 2016.
- 693
- 694 Brun F., Berthier, E., Wagnon, P., Kääb, A., and Treichler, D. : A spatially resolved estimate of High
695 Mountain Asia glacier mass balances from 2000 to 2016, *Nat. Geosci.*, 10, 668–673, doi:
696 10.1038/ngeo2999, 2017.
- 697
- 698 Cuffey, K. ,and Paterson, W.S.B. : The physics of glaciers, 4th Ed., Academic Press, Amsterdam, 2010.
- 699
- 700 Dussailant, I., Berthier, E. , Brun, F., Masiokas, M., Hugonnet, R., Favier, V., Rabatel, A., Pitte, P., and
701 Ruiz, L. : Two decades of glacier mass loss along the Andes, *Nature Geoscience*, 12, 802-808. doi:
702 10.1038/s41561-019-0432-5, 2019.
- 703
- 704 Eckert, N., Baya, H., Thibert, E. , and Vincent, C. : Extracting the temporal signal from a winter and
705 summer mass-balance series: application to a six-decade record at Glacier de Sarennes, French Alps, *J.*
706 *Glaciol.*, 57, 134–150, 2011.
- 707
- 708 Fischer, A. : Glaciers and climate change: Interpretation of 50 years of direct mass balance of
709 Hintereisferner, *Global and Planetary Change* 71, 1-2: 13-26, 2010.
- 710
- 711 Gagliardini, O., Zwinger, T., Gillet-Chaulet, F., Durand, G., Favier, L., de Fleurian, B., Greve, R.,
712 Malinen, M., Martín, C., Råback, P., Ruokolainen, J., Sacchetti, M., Schäfer, M., Seddik, H., and Thies,
713 J. : Capabilities and performance of Elmer/Ice, a new-generation ice sheet model, *Geosci. Model Dev.*, 6,
714 1299-1318, doi:10.5194/gmd-6-1299-2013, 2013.
- 715
- 716 Gardelle J., Berthier, E. and Arnaud, Y. : Slight mass gain of Karakoram glaciers in the early twenty-first
717 century, *Nature Geosci* 5, 322–325 (2012). <https://doi.org/10.1038/ngeo1450>, 2012.
- 718



- 719 Gardner, A.S., Moholdt, G., Cogley, J.G., Wouters, B., Arendt, A.A., Wahr, J., Berthier, E., Pfeffer, T.,
720 Kaser, G., Hock, R., Ligtenberg, S.R.M., Bolch, T., Sharp, M., Hagen, J.O., van den Broeke, M. R., and
721 Paul, P.: A reconciled estimate of glacier contributions to sea level rise: 2003–2009, *Science*, 340, 6134,
722 852–857, <https://doi.org/10.1126/science.1234532>, 2013.
- 723
- 724 Gillet-Chaulet, F., Gagliardini, O., Seddik, H., Nodet, M., Durand, G., Ritz, C., Zwinger, T., Greve, R.
725 and Vaughan, D. G. : Greenland ice sheet contribution to sea-level rise from a new-generation ice-sheet
726 model, *The Cryosphere*, 6(6), 1561–1576, doi:10.5194/tc-6-1561-2012, 2012.
- 727
- 728 Hantz, D., and Lliboutry, L. : Waterways, ice permeability at depth and water pressures at glacier
729 d’Argentière, French Alps, *J. Glaciol.*, Vol. 29, no. 102, 227–238, 1983.
- 730
- 731 Hock, R., Jansson, P. , and Braun, L. : Modelling the response of mountain glacier discharge to climate
732 warming. In Huber, U. M., Reasoner, M. A., and Bugmann, H. (eds.), *Global Change and Mountain*
733 *Regions - A State of Knowledge Overview*. Dordrecht: Springer, 243–252, 2005.
- 734
- 735 Hoelzle, M. Azisov, E., Barandun, M., Huss, M., Farinotti, D., Gafurov, A., Hagg, W., Kenzhebaev, R.,
736 Kronenberg, M., Machguth, H., Merkushkin, A., Moldobekov, B., Petrov, M., Saks, T., Salzmann, N.,
737 Schöne, T., Tarasov, Y., Usabaliev, R., Vorogushyn, S. and Zemp, M. : Re-establishing glacier monitoring
738 in Kyrgyzstan and Uzbekistan, Central Asia. *Geoscientific Instrumentation, Methods and Data Systems*.
739 6. 397–418. 10.5194/gi-6-397-2017, 2017.
- 740
- 741 Huss, M., and Bauder, A. : Twentieth-century climate change inferred from long-term point observations
742 of seasonal mass balance, *Ann. Glaciol.*, 50, 207–214, 2009.
- 743
- 744 Huss, M. : Present and future contribution of glaciers to runoff from macroscale drainage basins in
745 Europe, *Water Resources Research*, 47, W07511, doi:10.1029/2010WR010299. 2011.
- 746
- 747 Huss, M., Hock, R. , Bauder, A. , and Funk, M., : Conventional versus reference-surface mass balance,
748 *J. Glaciol.*, 58, 278–286, 2012.
- 749
- 750 Huss, M. , and Hock, R. : Global-scale hydrological response to future glacier mass loss. *Nat. Clim.*
751 *Chang.* 8, 135–140, 2018.
- 752
- 753 Immerzeel W. W., Pellicciotti, F. , and Bierkens, M.F. P. : Rising river flows throughout the twenty-first
754 century in two Himalayan glacierized watersheds, *Nat. Geosci.*, 6(9), 742–745, doi:10.1038/NGEO1896,
755 2013



756
 757 IPCC: IPCC Special Report on the Ocean and Cryosphere in a Changing Climate [H.-O. Pörtner, D.C.
 758 Roberts, V. Masson-Delmotte, P. Zhai, M. Tignor, E. Poloczanska, K. Mintenbeck, A. Alegría, M.
 759 Nicolai, A. Okem, J. Petzold, B. Rama, N.M. Weyer (eds.)], 2019.
 760
 761 Kraaijenbrink P.D.A., Immerzeel, W.W., Pellicciotti, F., de Jong, S.M., and Shea, J.M.: Object-based
 762 analysis of unmanned aerial vehicle imagery to map and characterise surface features on a debris-covered
 763 glacier, *Remote Sens. Environ.*, 186 (2016) 581–595, doi.org/10.1016/j.rse.2016.09.013, 2016.
 764
 765 Kaab, A. and Funk, M. : Modelling mass balance using photogrammetric and geophysical data: a pilot
 766 study at Griesgletscher, Swiss Alps, *J. Glaciol.*, 45,151, 575-583, 1999.
 767
 768 Kaser, G., Cogley, J.G., Dyurgerov, M.B., Meier, M.F. ,and Ohmura, A. : Mass balance of glaciers and
 769 ice caps: Consensus estimates for 1961–2004, *Geophys. Res. Lett.*, 33, L19501,
 770 doi:10.1029/2006GL027511, 2006.
 771
 772 Kaser, G., Grosshauser, M., and Marzeion, B. : Contribution potential of glaciers to water availability in
 773 different climate regimes, *Proceedings of the National Academy of Sciences of the United States of*
 774 *America*, 107(47): 20223-20227, 2010.
 775
 776 Leprince S., Ayoub, F., and Avouac, J.P. : Automatic and precise orthorectification, coregistration, and
 777 subpixel correlation of satellite images, application to ground deformation measurements. *IEEE Trans.*
 778 *Geosci. Remote Sens.*, **45**(6), 1529–1558, doi: 10.1109/TGRS.2006.888937, 2007.
 779
 780 Marzeion, B., Cogley, J.,G., Richter, K., Parkes, D. : Attribution of global glacier mass loss to
 781 anthropogenic and natural causes, *Science*, 22 August 2014, Vol. 345, Issue 6199, 919-
 782 921, DOI:10.1126/science.1254702, 2014.
 783
 784 Nienow, P.W., Hubbard, A.L., Hubbard, B.P., Chandler, D.M., Mair, D.W.F., Sharp, M.J. and Willis,
 785 I.C.: Hydrological controls on diurnal ice flow variability in valley glaciers, *J. Geophys. Res.*, 110,
 786 doi:10.1029/2003JF000112, 2005.
 787
 788 Paul, F., and Haeberli, W. : Spatial variability of glacier elevation changes in the Swiss Alps obtained
 789 from two digital elevation models, *Geophys. Res. Lett.*, 35, L21502, doi:10.1029/2008GL034718, 2008.
 790



791 Rabatel, A., Sanchez, O., Vincent, C., and Six, D. : Estimation of Glacier Thickness From Surface Mass
792 Balance and Ice Flow Velocities: A Case Study on Argentière Glacier, France, *Front. Earth Sci.* 6:112.
793 doi: 10.3389/feart.2018.00112, 2018

794

795 Rasmussen, L. A. : Altitude variation of glacier mass balance in Scandinavia, *Geophys. Res. Lett.*, 31,
796 L13401, doi:10.1029/2004GL020273, 2004.

797

798 Soruco, A., Vincent, C., Francou, B., and Gonzalez, J. F. : Glacier decline between 1963 and 2006 in the
799 Cordillera Real, Bolivia. *Geophysical Research Letters*, 36, L03502. <https://doi.org/10.1029/2008GL036238>,
800 2009.

801

802 Sugiyama, S. and Gudmunsson, G.H. : Short-term variations in glacier flow controlled by subglacial
803 water pressure at Lauteraargletscher, Bernese Alps, Switzerland, *J. Glaciol.*, 50 (170), 353-363, 2004.

804

805 Thibert E., Blanc, R. , Vincent, C., Eckert, N.: Glaciological and volumetric mass balance measurements:
806 error analysis over 51 years for Glacier de Sarennes, French Alps, *J. Glaciol.*, 54 (186), 522-532, 2008.

807

808 Thibert, E., Eckert, N. , and Vincent, C. : Climatic drivers of seasonal glacier mass balances: an analysis
809 of 6 decades at Glacier de Sarennes (French Alps), *The Cryosphere*, 7, 47–66. doi:10.5194/tc-7-47-
810 2013, 2013.

811

812 Thibert, E., Dkengne Sielenou, P., Vionnet, V., Eckert, N., and Vincent, C.: Causes of glacier melt
813 extremes in the Alps since 1949, *Geophys. Res. Letters*, 45, <https://doi.org/10.1002/2017GL076333>,
814 2018.

815

816 Vincent C. : Influence of climate change over the 20th Century on four French glacier mass balances.
817 *Journal of Geophysical Research*, 107, D19, ACL 4, 1-12, 2002.

818

819 Vincent, C., Kappenberger, G., Valla, F., Bauder, A., Funk, M., and Le Meur, E. : Ice ablation as evidence
820 of climate change in the Alps over the 20th century, *J. Geophys. Res.*, 109, D10104,
821 doi:10.1029/2003JD003857, 2004.

822

823 Vincent , C., Soruco, A. , Six, D. , and Le Meur, E. : Glacier thickening and decay analysis from fifty
824 years of glaciological observations performed on Argentière glacier, Mont-Blanc area, France, *Annals of*
825 *Glaciology*, 50, 73-79, 2009.

826



- 827 Vincent C., Fischer, A., Mayer, C., Bauder, A., Galos, S. P., Funk, M., Thibert, E., Six, D., Braun, L.,
828 and Huss, M. : Common climatic signal from glaciers in the European Alps over the last 50 years,
829 *Geophysical Research Letters*, 44. [https://doi:10.1002/ 2016GL072094](https://doi.org/10.1002/2016GL072094), 2017.
- 830
- 831 Vincent, C., Dumont, M. , Six, D. , Brun, F. , Picard, G., and Arnaud, L. : Why do the dark and light
832 ogives of Forbes bands have similar surface mass balances ? *J. of Glaciology*. *Doi:10.1017/jog.2018.12*,
833 *2018a*.
- 834
- 835 Vincent, C., Soruco, A., Azam, M. F., Basantes-Serrano, R., Jackson, M., Kjølmoen, B., Thibert, E. ,
836 Wagnon, P. , Six, D. , Rabatel, A. , Ramanathan, A. , Berthier, E. , Cusicanqui, D. , Vincent, P. , and
837 Mandal, A. : A nonlinear statistical model for extracting a climatic signal from glacier mass balance
838 measurements, *J. of Geophys. Res.: Earth Surface*, 123. [https://doi. org/10.1029/2018JF004702](https://doi.org/10.1029/2018JF004702), 2018b.
- 839
- 840 Wagnon P., Vincent, C. , Arnaud, Y., Berthier, E., Vuillermoz, E. , Gruber, S., Ménégoz, M., Gilbert, A.,
841 Dumont, M., Shea, J. M., Stumm, D., and Pokhrel, B. K.: Seasonal and annual mass balances of Mera
842 and Pokalde glaciers (Nepal Himalaya) since 2007, *The Cryosphere*, 7, 1769–1786, doi:10.5194/tc-7-
843 1769-2013, 2013.
- 844
- 845 World Glacier Monitoring Service (WGMS) *Global Glacier Change Bulletin No. 2. (2014–2015)*
846 (WGMS, 2017) <https://doi.org/10.5904/wgms-fog-2017-10>, 2017
- 847
- 848 Zemp, M., Huss, M., Thibert, E. *et al.*: Global glacier mass changes and their contributions to sea-level
849 rise from 1961 to 2016, *Nature* **568**, 382–386 , <https://doi.org/10.1038/s41586-019-1071-0>, 2019.